Electronic supplementary information (ESI)

Enhanced Energy Harvesting by Concentration Gradient-Driven Ion Transport in SBA-15 Mesoporous Silica Thin Films

Junho Hwang[a,b], Sho Kataoka[b,c], Akira Endo[b,c] and Hirofumi Daiguji[a,b]*

[a]Department of Mechanical Engineering, Graduate School of Engineering, The University of Tokyo, 7-3-1 Hongo, Bunkyo-ku, Tokyo 113-8656, Japan

[b]CREST, Japan Science and Technology Agency (JST), 7 Gobancho, Chiyoda-ku, Tokyo 102-0076, Japan

[c]National Institute of Advanced Industrial Science and Technology (AIST), AIST Tsukuba Central 5-2, 1-1-1 Higashi, Tsukuba, Ibaraki 305-8565, Japan

Table of Contents

S1. Fabrication of the nanofluidic device with an SBA-15 MPS thin film

The nanofluidic device was fabricated by bonding the microstructured-PDMS chip embossed by the soft lithography (Replica micromolding) to the Si chip on which a patterned MPS thin film was covered with a SiO_2 layer resulting in two reservoirs formed on both sides of the patterned MPS thin film. Fig. S1 shows a schematic illustration of the fabrication procedure for the nanofluidic device which has a built-in MPS thin film with uniaxially aligned nanopores.

Firstly, the as-prepared MPS thin film on the Si substrate (Stage 1) was covered with a positive photoresist (OFPR-800 30cP, Tokyo Ohka Kogyo Co., Ltd., Japan) layer of ~ 6.5 μm using a spin-coating method, then exposed by maskless arbitrary optical micro-pattern generator to form the rectangular pattern (1 mm in length ×300 μm in width), and developed in an aqueous alkali solution (NMD-3, Tokyo Ohka Kogyo Co., Ltd., Japan) for 90 s to obtain an upper layer pattern (Stage 2). In the following plasma chemical vapor deposition process (Stage 5), some deposits may be created inside the nanopores. To truncate the edge of the nanopore array, the width of the rectangular pattern here is larger than that of the final rectangular patterned MPS (1 mm in length × 100 μm in width). The resulting upper photoresist layer pattern was hard baked at 383 K for 300 s to produce a robust masking layer. Then, the rectangular mask patterned MPS thin film was formed by CF_4/O_2 plasma reactive ion etching, RIE, (SAMCO RIE-200L, Japan) at 80 W and 5 Pa for 60 s (Stage 3). Afterwards, the remaining photoresist layer was stripped off using an acetone remover (Wako Pure Chemistry Industries, Ltd., Japan) (Stage 4), then it was rinsed with DI water in the ultrasonic bath for 3 min, and the sample was hard baked at 383 K for 300 s again.

Secondly, a SiO_2 layer of ~100 nm in thickness was deposited onto the entire area including the patterned MPS thin film via plasma chemical vapor deposition, PCVD, (SAMCO PCVD PD-20SS, Japan) (Stage 5). Subsequently, the aforementioned mask pattern process on the substrate with the deposited SiO_2 thin layer was completed to make two reservoirs (1 mm in width × 3 mm in length) on

both sides of the patterned rectangular MPS thin film in the same way. The distance between reservoirs is 100 μm and identical with the width of the final rectangular pattern (Stage 6). The RIE process was then performed in the CF_4/O_2 plasma at 80 W and 5 Pa for 120 s to etch the deposited SiO_2 layer (Stage 7) and sequentially in the SF_6/O_2 plasma at 80 W and 5 Pa for 480 s to etch a layer of ~ 1 μm in depth on the Si substrates (Stage 8). Afterwards, the remaining photoresist layer was stripped off using the acetone remover (Stage 9), then it was rinsed with DI water in the ultrasonic bath for 3 min, and the sample was hard baked at 383 K for 300 s again.

Finally, the 1st microstructured-PDMS chip and 2nd PDMS chip for injecting aqueous solutions were bonded onto the patterned substrate with the MPS thin film by a wet-PDMS bonding method (Stage 10).

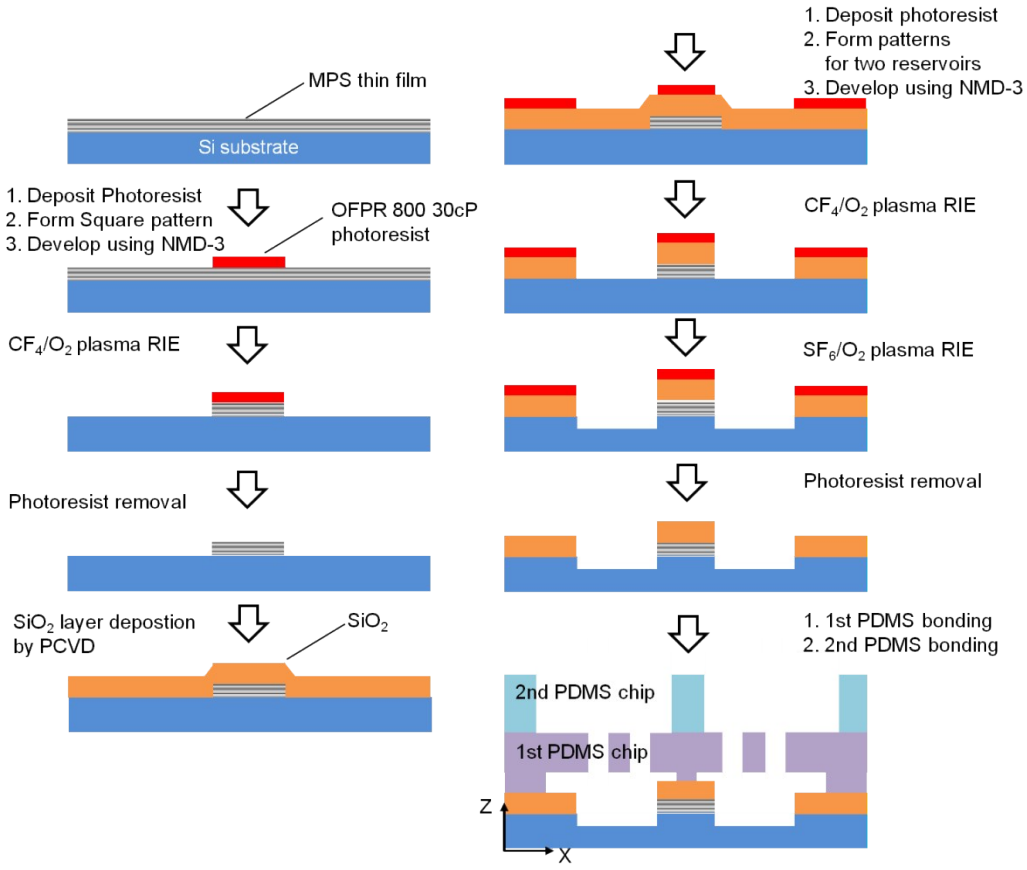

Figure S1. Schematic illustration of the fabrication procedure of the nanofluidic device with the MPS thin film of the uniaxially aligned nanopores.

Fig. S2 (a) and (b) show a top view and a cross-sectional view of PDMS chips produced by the soft lithography (replica micro-molding method), respectively. There are four holes (1 mm in diameter) for effectively injecting aqueous solutions. Two inlet holes were formed on each reservoir using a 1 mm-diameter disposable biopsy punch with a plunger system (Kai Industries Co. Ltd., Japan). The size of each reservoir is 3 mm in length, 1 mm in width, and 100 μm in height. The distance between the two reservoirs is 50 μm. The second PDMS chip shown in Fig. S2 (c) and (d) has much larger reservoirs and the size is 8 mm in length, 3.5 mm in width, and 5 mm in height.

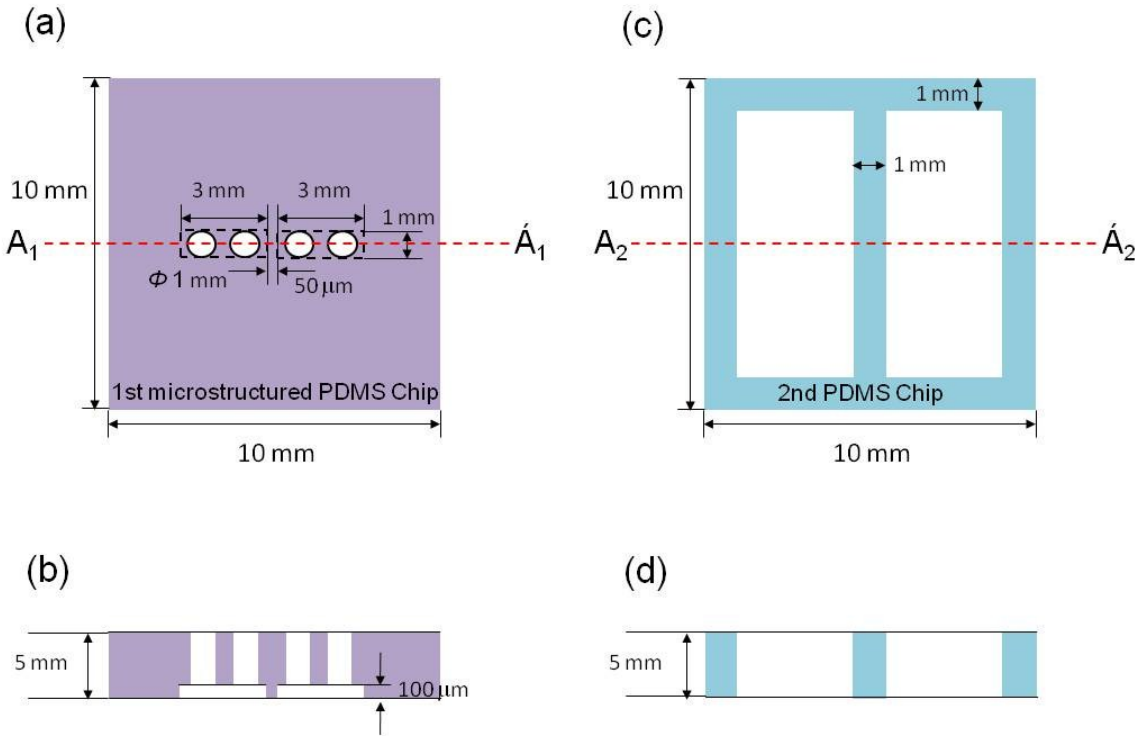

Figure S2. Schematic diagram of the PDMS chip. (a) Top view and (b) cross sectional view (at A_1-$Á_1$ line) of the first microstructured PDMS chip with four drilled holes for injecting aqueous solutions, and (c) top view and (d) cross-sectional view (at A_2-$Á_2$ line) of the second PDMS chip with two rectangular reservoirs.

The as-prepared PDMS chips were cleaned with isopropanol (Wako Pure Chemistry Industries, Ltd., Japan) in the ultrasonic bath for 600 s. The sample was dried using a nitrogen gun and then placed in a clean room at room temperature for 24 hours. Afterwards, a PDMS monomer/curing agent mixture (10:1 wt/wt %) was spread on a clean silicon substrate by a spin coater at 7500 rpm for 120 s, yielding a thin layer of wet PDMS (ca. 5 μm in thickness). The bonding side of the PDMS chip was directly applied to the wet PDMS layer, and thus the bonding surface was coated with the wet PDMS. Within half an hour, the PDMS chips were carefully aligned and bonded onto the patterned substrate using a stereomicroscope (model SMZ-1000, Nickon Instruments Inc., Japan) and a micro manipulator (M-152 model, Narishige, Japan). The combined chip was then cured in a convection oven at 353 K for 1 hour to completely seal the whole device.

S2. Equivalent circuit model for energy harvesting characteristics

Fig. S3 (a) shows the equivalent circuit representing the experimental setup. The electric potential generated in nanopores, V, is given by

$$V = V_{out} - V_{redox} = V_{oc} - IR, \quad \text{(S1)}$$

where I is the ionic current, V_{out} is the voltage output from a source meter, V_{redox} is the potential difference between two Ag/AgCl electrodes due to the redox reactions, V_{oc} is the open-circuit voltage due to the ion-selective property, and R is internal resistance of nanopores, respectively. V_{redox} is caused by an unequal potential drop at the two electrodes and given by the Nernst equation:[S1]

$$V_{redox} = \frac{RT}{zF} \ln \frac{\gamma_{c_H} c_H}{\gamma_{c_L} c_L}, \quad \text{(S2)}$$

where R, T, z, F, and γ are the gas constant, temperature, valence, Faraday constant, and activity coefficient, respectively. In this study, V_{redox} was measured using different combinations of c_H and c_L and the measured value was compared to the calculated one from Eq. S2. (Supporting Information S3)

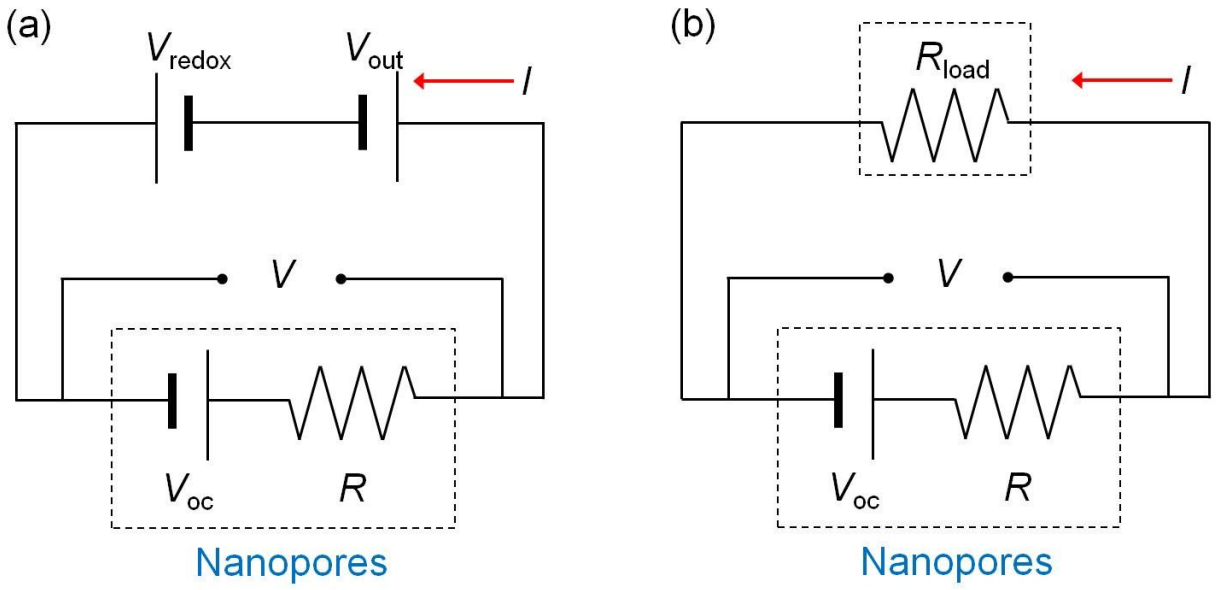

Figure S3. (a) Circuit model for the experimental setup and (b) the equivalent circuit model replacing the source meter (V_{out}) and the electrode (V_{redox}) with the electrical load (R_{load}).

V_{oc} satisfies the following equation:

$$V_{oc} = (2t_+ - 1)\frac{RT}{zF}\ln\frac{\gamma_{c_H} c_H}{\gamma_{c_L} c_L}, \quad \text{(S3)}$$

where t_+ is the transference number for the cation. From Eqs. S3 and S4, t_+ is given by

$$t_+ = \frac{1}{2}\left(\frac{V_{oc}}{V_{redox}} + 1\right). \quad \text{(S4)}$$

The transference number represents the ratio of the cation flux to the entire ion flux, i.e. $t_+ = J_+/(J_+ + J_-)$. Here, J_+ and J_- are the cation and anion fluxes, respectively. Note that $t_+ = 1$ and $t_+ = 0$ indicate either entirely cation or anion selective nanopores, respectively, while $t_+ \approx 0.5$ means non ion-selective nanopores if $D_+ \approx D_-$. If the energy harvesting system is composed of entirely cation-selective nanopores, i.e. $t_+ = 1$, then $V_{oc} = V_{redox}$ and V_{oc} becomes the maximum. Furthermore, if the source meter (V_{out}) and the electrode (V_{redox}) are regarded as the electrical load (R_{load}) for the energy harvesting system as shown in Fig. S3 (b), R_{load} is defined as follows:

$$R_{load} = \frac{V_{out} - V_{redox}}{I} = \frac{V}{I}. \quad \text{(S5)}$$

The power, P, is therefore given by

$$P = VI = V_{oc}^2 \frac{R_{load}}{(R_{load} + R)^2}. \quad \text{(S6)}$$

The maximum power, P_{max}, is obtained at $R_{load} = R$. Therefore, P_{max} is given by

$$P_{max} = \frac{V_{oc}^2}{4R}. \quad \text{(S7)}$$

When $P = P_{max}$, $V = V_{oc}/2$. The energy conversion efficiency, η, is defined as the ratio of the electrical output energy to the input energy, and given by[S2]

$$\eta = \frac{VI}{RT \ln\left(\frac{\gamma_{c_H} c_H}{\gamma_{c_L} c_L}\right) \int (J_+ + J_-) dA} . \quad \text{(S8)}$$

From Eqs. S1 and S3, the maximum energy conversion efficiency, η_{max}, is given by

$$\eta_{max} = \frac{(2t_+ - 1)I}{2zF \int (J_+ + J_-) dA} . \quad \text{(S9)}$$

Because the ionic current passing through nanopores is defined as $I = zF \int (J_+ - J_-) dA$, η_{max} can also be given by

$$\eta_{max} = \frac{1}{2}(2t_+ - 1)^2 . \quad \text{(S10)}$$

S3. Measurement of redox potential difference

To calibrate the electrodes, the measured V_{redox} using an electrochemical cell system was compared to the calculated value of Eq. S2. Activity coefficients in Eq. S2 were calculated with the Pitzer model (Supporting Information S4). In the measurement of V_{redox}, qualitative filter papers (ADVANTEC No.1 type, Toyo Roshi Kaisha, Ltd., Japan) were used as the salt bridge. The filter papers are 200 μm thick and retain coarse and gelatinous precipitates 10 μm in size. Here, the measured electric potential between two Ag/AgCl electrodes was attributed only to the asymmetric redox reactions at the electrode-solution interface. Fig. S4 shows the measured and calculated V_{redox} as a function of $\log(c_H/c_L)$. The measured and calculated V_{redox} were close to each other but the measured V_{redox} was slightly smaller than the calculated one. The measured and calculated V_{redox} of three kinds of electrolytes KCl, NaCl and LiCl are summarized in Table S1.

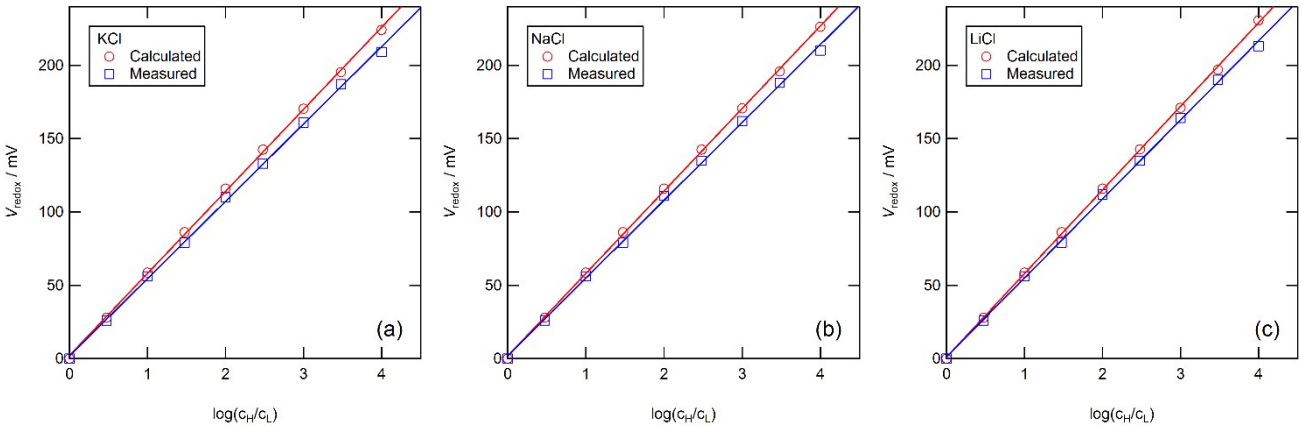

Figure S4. Measured and calculated V_{redox} as a function of $\log(c_H/c_L)$ for three kinds of electrolytes, (a) KCl, (b) NaCl, and (c) LiCl. The solid lines represent the fitting lines.

Table S1. Measured and calculated V_{redox} for the three electrolytes: KCl, NaCl, and LiCl.

(a) KCl

$\frac{c_H[M]}{c_L[M]}$	$\frac{3\times10^{-4}}{10^{-4}}$	$\frac{10^{-3}}{10^{-4}}$	$\frac{3\times10^{-3}}{10^{-4}}$	$\frac{10^{-2}}{10^{-4}}$	$\frac{3\times10^{-2}}{10^{-4}}$	$\frac{10^{-1}}{10^{-4}}$	$\frac{3\times10^{-1}}{10^{-4}}$	$\frac{10^{-0}}{10^{-4}}$
Calculated V_{redox} [mV]	28	58.6	86.2	116	142	171	195	224
Measured V_{redox} [mV]	26	56	79	110	133	161	187	209

(b) NaCl

$\frac{c_H[M]}{c_L[M]}$	$\frac{3\times10^{-4}}{10^{-4}}$	$\frac{10^{-3}}{10^{-4}}$	$\frac{3\times10^{-3}}{10^{-4}}$	$\frac{10^{-2}}{10^{-4}}$	$\frac{3\times10^{-2}}{10^{-4}}$	$\frac{10^{-1}}{10^{-4}}$	$\frac{3\times10^{-1}}{10^{-4}}$	$\frac{10^{-0}}{10^{-4}}$
Calculated V_{redox} [mV]	28	58.6	86.2	116	142	171	196	226
Measured V_{redox} [mV]	26	56	79	111	135	162	188	210

(c) LiCl

$\frac{c_H[M]}{c_L[M]}$	$\frac{3\times10^{-4}}{10^{-4}}$	$\frac{10^{-3}}{10^{-4}}$	$\frac{3\times10^{-3}}{10^{-4}}$	$\frac{10^{-2}}{10^{-4}}$	$\frac{3\times10^{-2}}{10^{-4}}$	$\frac{10^{-1}}{10^{-4}}$	$\frac{3\times10^{-1}}{10^{-4}}$	$\frac{10^{-0}}{10^{-4}}$
Calculated V_{redox} [mV]	28	58.6	86.2	116	143	171	197	231
Measured V_{redox} [mV]	26	56	79	112	135	164	190	213

S4. Activity coefficients for calculating the redox potentials

When the concentration of aqueous solutions is less than 2 mM, the activity coefficients are approximated by the Debye-Hückel limiting law:[S3]

$$\log \gamma_{\mathrm{i}} = -Az_{\mathrm{i}}\sqrt{I} \ . \quad \text{(S11)}$$

Here, γ_{i} and z_{i} are the activity coefficient and valence of ion species i, A is a constant which depends on temperature and an experimental value of water = 0.509 $\mathrm{mol}^{-1/2}$ $\mathrm{kg}^{1/2}$ at 298 K, and I is the ionic strength for electrolytes defined by $I = \frac{1}{2}\sum_{\mathrm{i}} c_{\mathrm{i}} z_{\mathrm{i}}^2$, where c_{i} is the molar concentration of ion species i. However, in this study, the concentration ranges from 0.1 mM to 1 M, thus the Debye- Hückel limiting law is not applicable and the Pitzer model is used instead to determine the activity coefficients in the high ionic strength solutions ($\leq$ 1 M). In the Pitzer model, the activity coefficients of aqueous solutions at 298 K are given by the following equations:[S4-S6]

$$\ln \gamma_{\mathrm{M}} = z_{\mathrm{M}}^2 f^{\gamma} + 2\sum_{\mathrm{X}} c_{\mathrm{X}} G_{\mathrm{MX}} + \sum_{\mathrm{M}}\sum_{\mathrm{X}} c_{\mathrm{M}} c_{\mathrm{X}} G'_{\mathrm{M}} \ , \quad \text{(S12)}$$

$$\ln \gamma_{\mathrm{X}} = z_{\mathrm{X}}^2 f^{\gamma} + 2\sum_{\mathrm{M}} c_{\mathrm{M}} G_{\mathrm{MX}} + \sum_{\mathrm{M}}\sum_{\mathrm{X}} c_{\mathrm{M}} c_{\mathrm{X}} G'_{\mathrm{X}} \ , \quad \text{(S13)}$$

where the subscript M and X refer to cations and anions, respectively, and f^{γ} is the electrostatic term. At a fixed valence, f^{γ} is the same for all kinds of ions, and given by

$$f^{\gamma} = -A^{\phi}\left\{\frac{\sqrt{I}}{\left(1+b\sqrt{I}\right)} + \frac{2}{b}\ln\left(1+b\sqrt{I}\right)\right\}, \quad \text{(S14)}$$

where b is a constant and assumed to be 1.2 and A^{ϕ} is the Debye-Hückel coefficient for the osmotic function, and given by

$$A^{\phi} = \frac{2\pi N_{\mathrm{A}} \rho_{\mathrm{w}}^{1/2}}{3\times 10^3}\left(\frac{e^2}{\varepsilon k_{\mathrm{B}} T}\right)^{3/2} , \quad \text{(S15)}$$

where N_A is the Avogardo number, ρ_w and ε are the density and the dielectric constant of pure solvent, k_B is the Boltzmann constant, and e is the electric charge. The parameters G_{MX}, G'_M and G'_X in Eqs. S11 and S12 are given by

$$G_{MX} = B_{MX} + \frac{1}{2}\left(\sum_i c_i |z_i|\right) C_{MX}, \quad \text{(S16)}$$

$$G'_M = z_M^2 B'_{MX} + z_M C_{MX}, \quad \text{(S17)}$$

$$G'_X = z_X^2 B'_{MX} + |z_X| C_{MX}, \quad \text{(S18)}$$

where C_{MX} is given by

$$C_{MX} = \frac{C^{\phi}_{MX}}{2\sqrt{|z_M z_X|}}. \quad \text{(S19)}$$

For 1:1 electrolyte, the parameters of B_{MX} and B'_{MX} are given by

$$B_{MX} = \beta^{(0)}_{MX} + \frac{2\beta^{(1)}_{MX}}{\alpha^2 I}\left\{1 - \left(1 + \alpha\sqrt{I}\right)\exp\left(-\alpha\sqrt{I}\right)\right\}, \quad \text{(S20)}$$

$$B'_{MX} = \frac{2\beta^{(1)}_{MX}}{\alpha^2 I^2}\left\{-1 + \left(1 + \alpha\sqrt{I} + \frac{1}{2}\alpha^2 I\right)\exp\left(-\alpha\sqrt{I}\right)\right\}, \quad \text{(S21)}$$

where α is a constant and assumed to be 2.0. The interaction parameters of C^{ϕ}_{MX}, $\beta^{(0)}_{MX}$ and $\beta^{(1)}_{MX}$ are summarized in Table S2.

Table S2. The interaction parameters of C^{ϕ}_{MX}, $\beta^{(0)}_{MX}$ and $\beta^{(1)}_{MX}$ for KCl, NaCl and LiCl electrolytes.[S6]

Electrolyte	C^{ϕ}_{MX}	$\beta^{(0)}_{MX}$	$\beta^{(1)}_{MX}$
KCl	-0.00084	0.04835	0.2122
NaCl	0.00127	0.0765	0.2664
LiCl	0.1494	0.3074	0.00359

Fig. S5 shows the activity coefficients for three kinds of electrolytes: KCl, NaCl and LiCl calculated by the Pitzer model. The calculated values of the activity coefficients are summarized in Table S3.

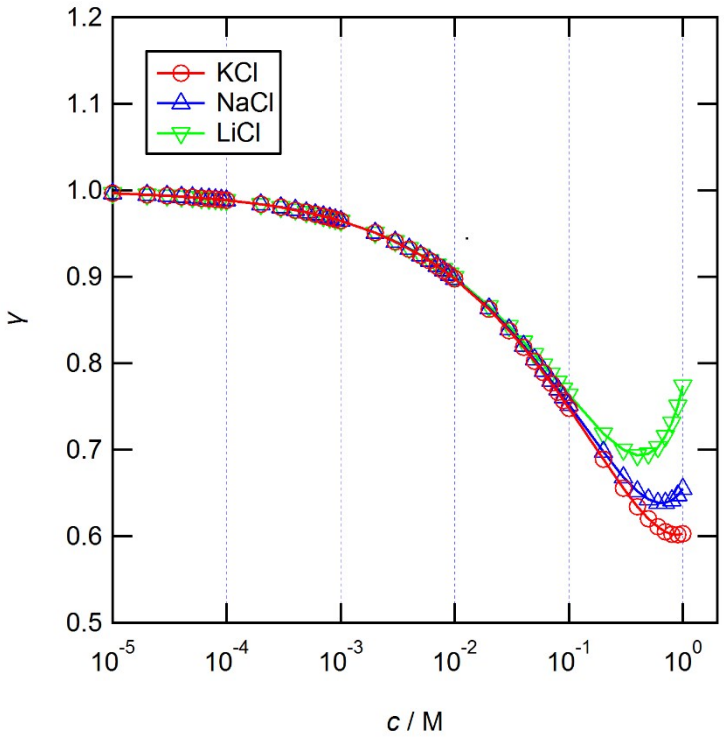

Figure S5. Activity coefficients with respect to the concentrations for the three electrolytes: KCl, NaCl, and LiCl.

Table S3. Calculated values of the activity coefficients.

Concentration [M]	KCl	NaCl	LiCl
10^{-4}	0.988	0.988	0.988
3×10^{-4}	0.980	0.980	0.980
10^{-3}	0.964	0.965	0.965
3×10^{-3}	0.940	0.941	0.941
10^{-2}	0.897	0.898	0.899
3×10^{-2}	0.838	0.839	0.843
10^{-1}	0.748	0.752	0.763
3×10^{-1}	0.656	0.668	0.700
1	0.603	0.655	0.774

S5. Effect of weak ion concentration solutions on p_{max} and η_{max}

Fig. S6 shows the p_{max} and η_{max} with respect to $\log(c_H/c_L)$ for KCl. The higher concentration (c_H) was fixed at 100 mM and the lower concentration (c_L) gradually increased from 0.3 to 30 mM. The lower concentration (c_L) was the variable in this experiment. The measured and calculated V_{redox} values with respect to c_H/c_L are summarized in Table S4. In comparing Fig. S6 to Fig. 8 (c) and (d), the highest values of p_{max} and η_{max} decrease with increasing c_L from 0.1 mM, but both values of p_{max} and η_{max} retain simultaneously high levels at $\log(c_H/c_L)$ = 1.5–2.5. The highest p_{max} is 2.85 W m^{-2} at $\log(c_H/c_L)$ = 2.5 and the highest η_{max} is 36.2% at $\log(c_H/c_L)$ = 1.5.

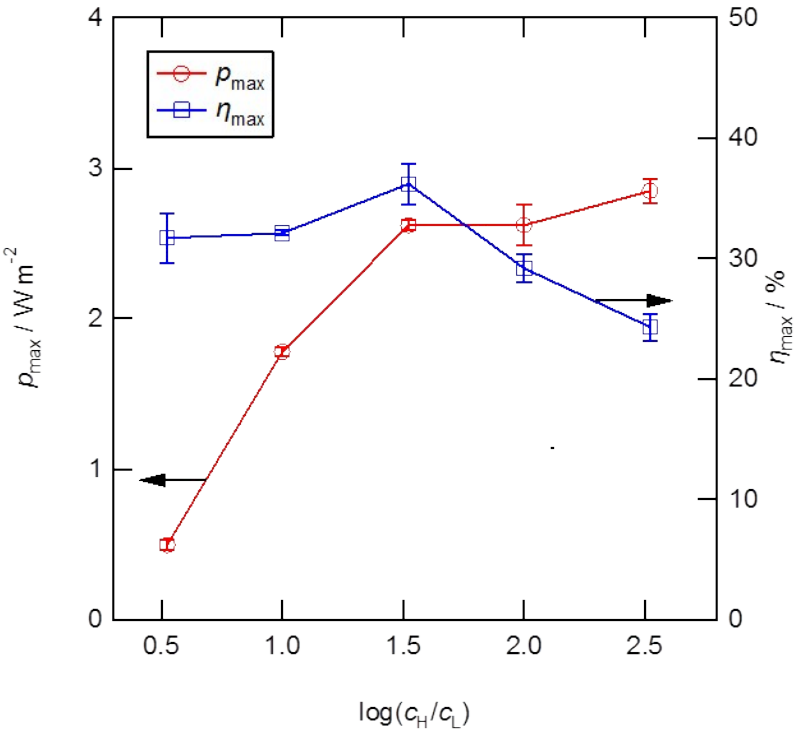

Figure S6. Power density and energy conversion efficiency with respect to different concentration gradients for KCl. The error bars represent the standard deviations.

Table S4. Measured and calculated V_{redox} of KCl.

$\frac{c_H[M]}{c_L[M]}$	$\frac{10^{-1}}{3\times10^{-4}}$	$\frac{10^{-1}}{10^{-3}}$	$\frac{10^{-1}}{3\times10^{-3}}$	$\frac{10^{-1}}{10^{-2}}$	$\frac{10^{-1}}{3\times10^{-2}}$
Calculated V_{redox} [mV]	142.4	111.9	84.3	54.5	28.1
Measured V_{redox} [mV]	134	107	79	53	27

References

S1 A. J. Bard and L. R. Faulkner, *Electrochemical Methods: Fundamentals and Applications*, John Wiley, New York, 2001

S2 J. C. Fair and J. F. Osterle, *J. Chem. Phys.*, 1971, **54**, 3307.

S3 P. Debye and E. Hückel, *Physikalische Zeitschrift*, 1923, **24,** 185.

S4 B. S. Krumgalz and F. J. Millero, *Mar. Chem.*, 1982, **11**, 209.

S5 K. S. Pitzer, *J. Phys. Chem.*, 1973, **77**, 268.

S6 K. S. Pitzer and G. Mayorga, *J. Phys. Chem.*, 1973, **77**, 2300.